Synergistic effect of surface states and deep defects for ultrahigh gain deep-ultraviolet photodetector with low-voltage operation

Keyun Gu[1,2], Kongping Wu[3], Zilong Zhang[1], Jian Huang[2], Mastaka Imura[1], Yasuo Koide[1], and Meiyong Liao[1*]

[1]National Institute for Materials Science, Namiki 1-1, Tsukuba, Ibaraki 305-0044, Japan

[2] School of Materials Science and Engineering, Shanghai University, Shanghai 200444, PR China

[3]School of Electronics and Information Engineering, Jinling Institute of Technology, Nanjing, 211169, Jiangsu, PR China

Correspondence to: Meiyong Liao* (meiyong.liao@nims.go.jp)

Abstract

To achieve ultra-high gain deep-ultraviolet (DUV) detectors based on ultra-wide bandgap semiconductors comparable with those of bulky photomultiplier tubes (PMTs), avalanche photodiodes (APDs) have usually been adopted. However, the high-operation voltage (~100 V) is not compatible with monolithic integration and hinders the broad applications. Herein, we demonstrate that the ultra-high gain DUV photodetectors (PDs) with low operation voltages (<5 V) can be achieved by using the synergistic effect of surface states and deep defects in a type-Ib single-crystal diamond (SCD) substrate. The overall photoresponse, such as the sensitivity, dark current, spectral selectivity, and response speed, of the diamond DUV-PDs can be simply tailored by the surface hydrogen or oxygen termination of the diamond containing deep nitrogen defect. The DUV responsivity and external quantum efficiency are more than $2.5\text{x}10^4$A/W and $1.4\text{x}10^7$%, respectively, at 220 nm-wavelength light, the highest among the DUV detectors and comparable with those of PMTs. The DUV/visible light rejection ratio ($R_{220\ nm}/R_{400\ nm}$) is as high as 6.7×10^5. The depletion of the two-dimensional hole gas on the hydrogen-terminated diamond surface by deep nitrogen defect provides a low background dark current and the filling of the ionized nitrogen upon DUV illumination induces a huge photocurrent. The synergistic effect of the surface states and the bulk deep defects opens the avenue for the development of DUV detectors with ultra-high sensitivity and low operation voltages compatible with integrated circuits.

Keywords: Ib-diamond, Deep defects, Solar blind photodetectors, Ultrahigh gain

1. Introduction

Solar blind deep-ultraviolet (DUV) photodetectors (PDs) are considered as a significant core of detection and communication covering civil and military due to their concealment and precision of photoelectric conversion in the 200-280 nm wavelength range [1, 2, 3]. Solar blind DUV PDs satisfying 5S requirements (high Sensitivity or responsivity, high Speed, high spectral Selectivity, high Signal-to-Noise ratio, and high Stability) [4] are in demand. The commercial photo-emissive devices (photomultiplier tubes-PMTs) can achieve high detectivity in the UV and visible light region, but they exhibit bulky volume, high-power consumption, vacuum requirement, high bias voltages, sensitivity to magnetic fields and low UV-visible light rejection ratio[5, 6, 7]. Lately, great efforts have been devoted to the development of DUV detectors with high photocurrent gain, essential for weak DUV light detection. The ultra-wide bandgap (UWBG) semiconductors such as Ga_2O_3, AlGaN, MgZnO, and diamond enable the development of solar-blind DUV PDs without the requirement of optical filters [8, 9, 10]. Recently, numerous solar-blind PDs were developed based on the UWBG semiconductors with varied structures and properties [11, 12, 13, 14, 15]. Despite the great progress in AlGaN growth methodology, the achievements of high-crystal quality Al-rich AlGaN and efficient p-type doping have remained a challenge yet due to the high dislocation density [16]. Therefore, the performance of the DUV PDs base on AlGaN are still far from that of the ideality. For $Mg_xZn_{1-x}O$, a Mg composition over 37% has the problem of phase segregation, degrading the photoresponse performance [17]. Ga_2O_3 has been emerged as the promising alternate for DUV photodetectors due to the facile synthesis [17, 18]. Nevertheless, the oxygen vacancy in Ga_2O_3 induces the background dark current and degrades the spectral selectivity. Despite these problems of the UWBG semiconductors, Ga_2O_3-based photodiodes with photocurrent gain over 10^5 was developed, which is an encouraging alternative to the photomultiplier tubes requiring vacuum condition [12]. However, to achieve high photocurrent gain, avalanche photodiode

(APD) structures generally have to be fabricated [19]. For UWBG semiconductors, the APDs raise the critical problem of high operation volage around 100 V, which is not facile for monolithic integration [12, 20, 21]. Another challenging issue for APD based on UWBGs is the fabrication of high-quality heterostructure interface to reduce the dark current for achieving the breakdown state. Diamond owns the highest thermal conductivity (22 $W \cdot cm^{-1} \cdot K^{-1}$), chemical inertness, high insulation, and high radiation resistance [22, 23, 24, 25, 26]. Up to date, a wide variety of diamond-based PDs have been developed, including Schottky diode [27, 28], heterojunction [29, 30], photoconductor [31, 32], and metal-semiconductor-metal structure [33, 34, 35]. In spite of continuous efforts devoted to enhancing the performance of diamond DUV PDs, the sensitivity still need to be improved and the overall performance need to be tailored based on application needs.

Here, we show that a solar-blind DUV photodetector with a responsivity over 2.5×10^4 A/W can be achieved at low voltage (5 V) by combining the synergistic effect of surface terminations and deep defects in diamond. A recorded external quantum efficiency (EQE) of 1.4×10^7 % under the DUV light (220 nm) illumination and a DUV/visible rejection ratio of 6.7×10^5 are achieved. The surface depletion under dark condition and recovery of the two-dimensional hole gas (2DHG) surface conductivity upon DUV illumination tailor the low dark current and ultra-high photocurrent gain, respectively. In addition, the operation voltage is over 10 times smaller than those of APDs, which is compatible for electrically monolithic integration. Our strategy is simply conducting a 30 min hydrogen (H)-plasma treatment of a commercialized high-pressure high-temperature (HPHT) type-Ib single-crystal diamond (SCD) substrate without the growth of a homoepitaxial diamond layer. We employ the simplest metal-semiconductor-metal (MSM) device configuration without the requirements of high-quality heterostructural interface and dedicated device design. In addition, the photoresponse properties such as the gain, response speed, and spectral selectivity can be tailored by a simple ozone treatment. The high-gain DUV detector is benefitted from the unique properties of the type-Ib diamond: (i) intrinsically no

stoichiometric compositional problem, (ii) a cut-off wavelength at 225 nm, (iii) ability to form a high density of 2DHG on the hydrogen-terminated diamond surface, (iv) lower dark current than intrinsic diamond with hydrogenated surface, and (v) donor type deep defect of nitrogen. The gain (10^5) of the diamond PD is comparable to those of PMTs despite the indirect bandgap structure of diamond.

2. Results and Discussion

2.1 Tailoring the surface band bending and conductivity of diamond with surface terminals

The surface terminals and components can be adjusted by different surface treatment including hydrogen plasma treatment and ozone treatment. We measured the surface components by X-ray Photoelectron Spectroscopy (XPS), as shown in **Figure S1(a1) (Supporting Information).** All samples exhibit a main peak around 284.80 eV, which corresponds to bulk sp3 C-C bonds. Ozone oxidation processes induce several kinds of C-O bond peaks around 287 eV[36], as shown in **Figure S1(a2) and (a3) (Supporting Information)**. Compared with the 15 min-ozone treated diamond, the diamond with 45 min- ozone treatment has more oxidized component. The C-O bonds of diamond treated with ozone for 15 minutes accounted for 2.90% and those treated with ozone for 45 minutes accounted for 5.85%. Furthermore, the energy band structure of the diamond surface can be tailored by surface terminations or surface states. When the H-terminated diamond is exposed to air, a high density 2DHG will be formed on the surface with a upward band bending [37]. The 2DHG is presently the mainstream p-channel for the fabrication of diamond field-effect transistors [38, 39, 40]. The high density 2DHG contributes to a large background dark current, in which the photocurrent is buried for an intrinsic H-terminated diamond surface. The sheet resistance of the PDs based on the intrinsic H-terminated diamond is typically ~kΩ/sq [37], much smaller than that (of GΩ /sq) of an oxidized diamond surface [41]. This is due to the strong negative electron affinity of intrinsic diamond (-2.47 eV), as show in **Figure S1(b1) (Supporting Information)**. Here, the

type-Ib SCD with [N]~ 10^{19} cm^{-3} and without intrinsic diamond epilayer was hydrogenated by using microwave plasma chemical vapor deposition (MPCVD) in a pure hydrogen plasma ambient. The conventional metal-semiconductor-metal (MSM) structure with interdigitated finger electrodes is utilized to fabricate the photodetectors. Both the finger electrode width and the figure space are 10 μm. By controlling the hydrogen plasma treatment durations, the surface conductivity can be modulated, as shown in **Figure S2**. For the 20 min H-plasma treatment, the dark current of the MSM-PD is around pA at 1 V, for the 30 min H-plasma treatment, the dark current of the PD is around μA at 1 V. The energy band of the H-terminated diamond with 30 min H-plasma treatment bend upward sharply and the surface has a higher negative electron affinity (NEA) [42, 43] (**Figure 1a**). Despite the 30 min H_2 plasma treatment, the 2DHG $D(h^+)_{total}$ is partially depleted, resulting in a reduction of the negative electron affinity (NEA) of -2.13 eVand dark current. The upward band bending or the NEA of the H-terminated surface on the type-Ib diamond substrate is supported by first-principles calculations (**Figure S1(b1) (Supporting Information).** The nitrogen in diamond as an electron donor in the typ-Ib diamond [44, 45] and compensates the surface holes, resulting in increasing the amount of N^+ deep trap ($D(N^+)$) in diamond and descending the density of total holes ($D(h^+)_{total}$). The total hole density is the sum of the surface remaining hole density ($D(h^+)_{surf}$) and the depleted density ($\Delta D(h^+)_{dep}$). The number of holes depleted on the hydrogen-terminated diamond surface is equal to the increase charged density of N^+. The equivalent relationship can be described by equations (1) and (2).

$$D(h^+)_{total} = D(h^+)_{surf} + \Delta D(h^+)_{dep} \quad (1)$$

$$\Delta D(h^+)_{dep} = D(N^+) \quad (2)$$

The dark current is consequently reduced to 9.8 μA at 1 V (**Figure 1d**), three to four orders of magnitude lower than that of the MSM device on an intrinsic H-terminated diamond surface. By controlling the ozone treatment duration, the dark current can be modulated. As the ozone treatment duration increases, the H-terminated diamond surface is gradually converted to

oxygen (O)-terminated one, effectively reducing the density of surface holes and the formation of charged nitrogen, bringing about the decrease of negative electron affinity (-0.96 eV) (**Figure S1(b2) (Supporting Information)**) and band bending upward gently and the reduction of $D(N^+)$, as shown in **Figure 1b**. Meanwhile, the dark current markedly drops to 1.4 pA at 1 V (**Figure 1e).** The enhancement of oxidation arouses less charge transfer of electrons from diamond to the surface adsorbates, reducing the number of surface holes and decreasing the dark current. The O-terminated diamond with an electron affinity of 2.62 eV (**Figure S1(b2) (Supporting Information)**) and electric dipole moment in the opposite direction [46] is obtained after the ozone treatment for 45 min, leading to the band bend downward (**Figure 1c**) and an extremely low current (~10^{-14} A) at the noise level of the analyzer (**Figure 1f**).

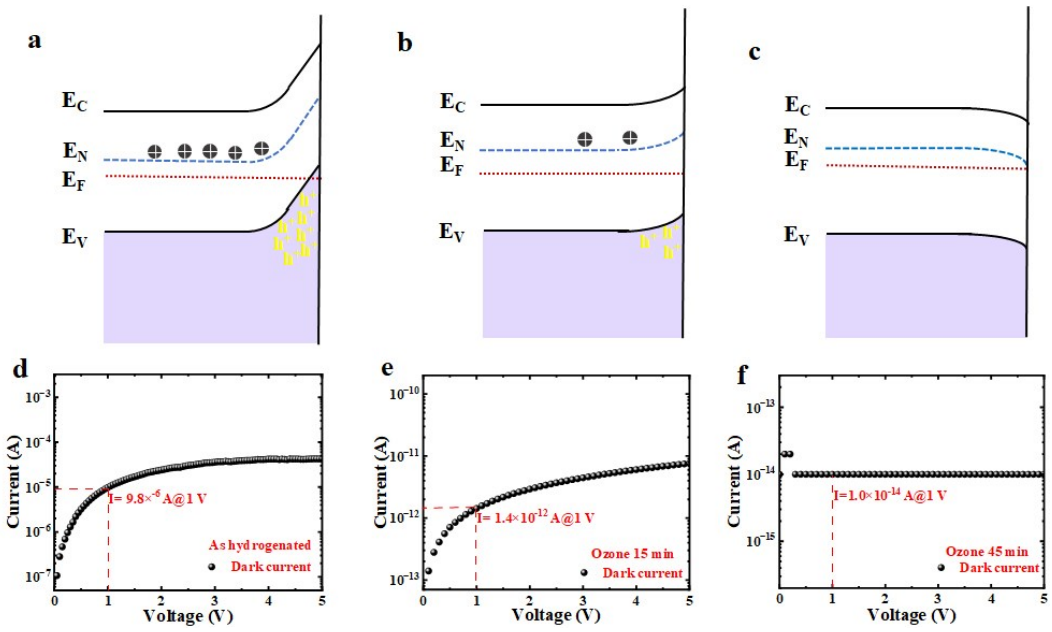

Figure 1. Energy band diagram and surface conductivity. a-c) Energy band diagram and d-f) dark current of H-terminated (30min H-plasma), partial H-terminated (ozone treatment for 15 min), and O-terminated (ozone treatment for 45 min) diamond-based PDs, respectively. The nitrogen-vacancy energy level is not illustrated in the band diagram.

2.2 Photo-response regulation

With the intention of investigating the tailoring-process of photoresponse characterizations of the PDs based on the type-Ib diamond with various surface states, a 220 nm-wavelength UV light (~20μW/cm^2) was utilized for the photoresponse measurement of the PDs with different oxidation degrees or ozone treatment durations. As shown in **Figure 2a**, the photocurrent of the PD based on H-terminated diamond boosts to an ultrahigh value of 2.9×10^{-4} A at 5 V instead of being buried, illustrating a remarkable response. As for the ozone treatment for 15 min, the current of the PD increases from 7.6×10^{-12} A in dark to 2.9×10^{-9} A under illumination at 5 V bias as depicted in **Figure 2b**. Compared with H-terminated diamond PD, the photocurrent of the PD with 15 min ozone treatment drops by five orders of magnitude. For the PD with O-terminated diamond surface (45 min ozone treatment), the photocurrent is two orders of magnitude higher than the dark current, reaching 1.3x 10^{-11} A as shown in **Figure 2c**. The overall photo-response trend of all PDs with various treatments is summarized in **Figure 2d**. In general, the photocurrent at the 220 nm-wavelength light of all PDs increases significantly compared to the dark current. Furthermore, the dark current and photo current are gradually descended as the degree of oxidation escalates, which is resulted from the oxidation reducing the surface 2DHG concentration. After 45 min ozone oxidation, the H-terminated diamond is converted to O-terminal diamond, so that the device has the lowest dark current and photocurrent.

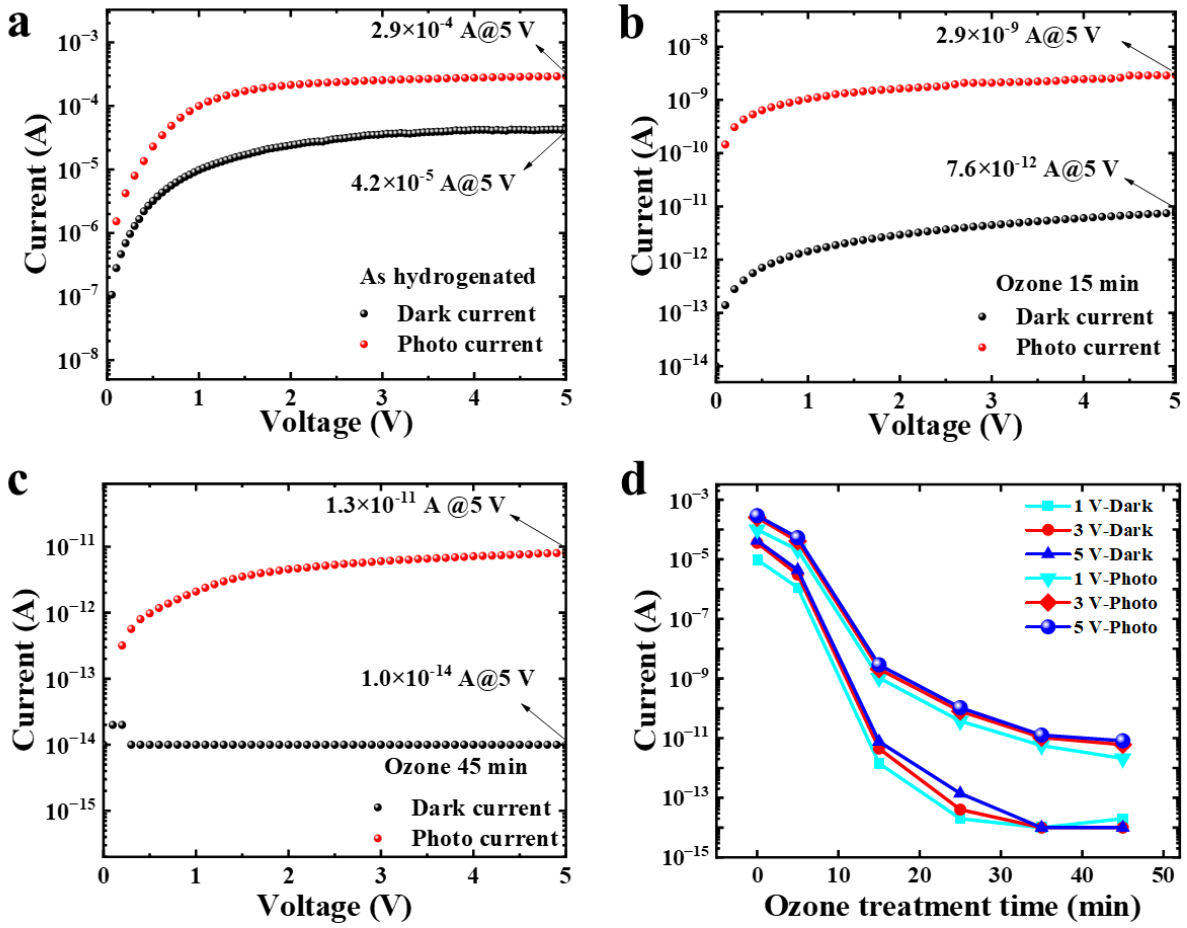

Figure 2. I-V characteristics of the photodetectors under dark and DUV light illumination. a) Hydrogenated. b) Ozone treatment of 15 min. c) Ozone treatment of 45 min. d) Tendency of dark and photo current of the type-Ib diamond-based solar blind PDs with different treatments.

The measured external quantum efficiency (EQE) of PDs with different treatment are shown in **Figure 3a**. The *EQE* value of the as hydrogenated detector reaches ~1.4×10^{7}% at 5 V, which is the highest among the DUV PDs. Furthermore, the EQE of PDs continue to decrease dramatically with the prolonged oxidation time: the EQE of the PD with 5 min ozone treatment drops to 2.8×10^{6}%, and the EQE is even reduced to 0.45% for the PD with 45 min ozone treatment. All the PDs exhibit higher EQE in DUV region and lower EQE in visible light region. Base on the measured EQE, the responsivity (R) of a PDs can be calculated according to the formula $R = EQE\frac{e\lambda}{hc}$. Where h represents Planck constant, c is light speed, e is electron charge,

and λ is the light wavelength [47], as shown in **Figure 3b**. The R is calculated to be as high as over 2.5x10^4 A/W at 5 V under the 220 nm light illumination for the as-hydrogenated diamond-based PD. After 5 min ozone treatment, the R of the PD decreases to 4.8x10^3 A/W. For PD treated with ozone for 15 minutes, its R drops by five orders of magnitude to 0.29 A/W compared to the as hydrogenated PD. As for the PD with 45 min ozone treatment, the value of R even decays to ~10^{-4} A/W. The rejection ratio of DUV/visible light is illustrated by R_{220nm}/ R_{400nm} as shown in the inset in **Figure 3b**. For the PDs based on the as hydrogenated diamond surface, the ratio reaches 6.7×10^5, suggesting an excellent spectral selectivity of solar blind region. As the oxidation level of the devices increases, the rejection ratio becomes lower, resulting in descending spectral selectivity to 10^4. The noise current vs. frequency (from 0.1 Hz to 100 Hz) of all PDs are shown in **Figure 3c.** The as-hydrogenated PD shows higher noise current of 1.8×10^{-7} A/$Hz^{1/2}$, while the PDs with 5min, 15 min, 25 min, 35 min, and 45 min ozone treatment time show 1.3×10^{-8} A/$Hz^{1/2}$, 5.2×10^{-13} A/$Hz^{1/2}$, 8.2×10^{-15} A/$Hz^{1/2}$, 6.1×10^{-15} A/$Hz^{1/2}$, 5.1×10^{-15} A/$Hz^{1/2}$, respectively. It is displayed that the noise current is dominated by the dark current. The specific detectivity (D*) is also an important parameter to measure the performance of the PD and directly reflects the PD's ability to detect weak signals, which is given by $D^* = \frac{R\sqrt{AB}}{I_n}$ [48]. Where the R is the responsivity, A is the effective detection area, B is the bandwidth, I_n is the measured total noise current. The calculated specific detectivity vs. wavelength is shown in **Figure 3d**. Due to the high noise current, the detectivity D* of the as-hydrogenated PD is degraded, which is 2.5×10^{10} cm $Hz^{1/2}$ W^{-1} . The suitable ozone treatment for 5 min reduces the noise current, thus improves the D* value to 1.4×10^{11} cm $Hz^{1/2}$ W^{-1} while maintaining a high EQE (2.8×10^6%,). While the PDs with 15 min, 25 min, 35 min, and 45 min ozone treatments show a D* value of ~10^{10} cm $Hz^{1/2}$ W^{-1}. All PDs exhibit higher D* in DUV region than visible light region.

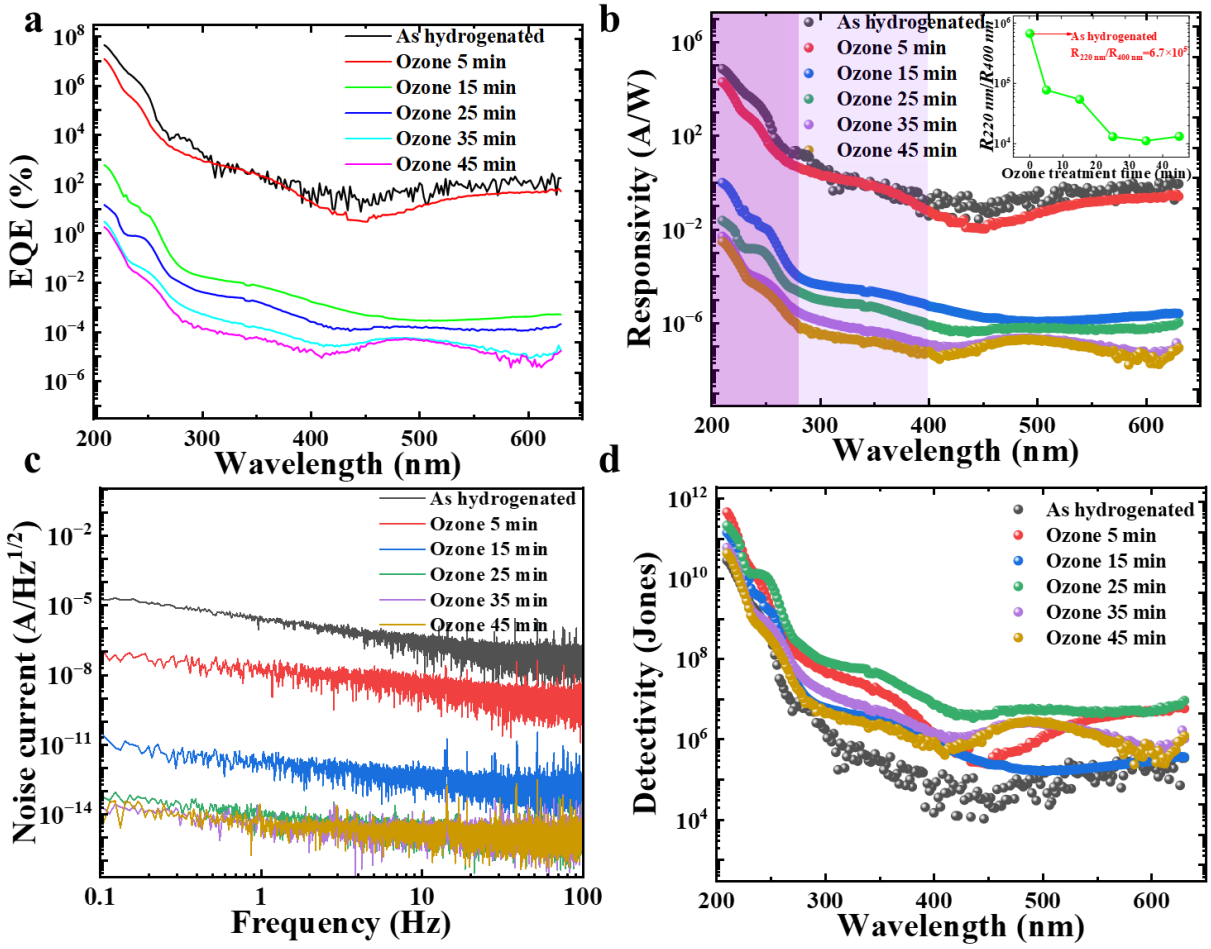

Figure 3. Photoresponse properties vs oxidation duration. a) Measured external quantum efficiency, *EQE*. b) Responsivity, *R* and UV/visible rejection ratio ($R_{220\ nm}/R_{400\ nm}$). c) Noise current and d) detectivity, d) *D** of PDs with different ozone treatment durations.

Finally, the time-dependent photoresponse was investigated. The current of the PDs rises to a value with light on and decreases with light off as shown in **Figure 4**, which is ascribed to the generation and recombination of photogenerated carries. The response time of the current PDs is a competitive process of the deep-traps of nitrogen in the type-Ib diamond substrate and the surface recombination centers. As for the as-hydrogenated PD, the ionized nitrogen traps due to surface holes on the H-terminatiation and air adsorptions dominate the overall photocurrent and response time. Since nitrogen level in diamond is deep (~1.7 eV below the conduction band), the PD of the as-hydrogenated diamond showed an increasing in photocurent with light

illumination due to the slow filling of the ionized nitrogen by photo-generated electronics. Therefore, the resonse time is slow. For the fully oxidized diamond surface, the surface recombination related to C-O or C=O bonds dominated the photocurrent, thus the response speed is fast. This can also explain the PDs after 5min-ozone treatment. The abnormal behavior of the 15min-ozone treated PD, the increase of the photocurrent over time, is unknown. The possible reason is that the 15min-treated PDs induces some low-density new deep electron traps like carbon bonded with oxygen and hydrogen, which surpasses the surface recombination centers. Besides, the rise time τ_r (10% to 90% of the maximum photocurrent) and the decay time τ_d (90% to 10% of the maximum photocurrent) were calculated. The as hydrogenated diamond-based device has a response rising time τ_r of 10.7 s and a decay time τ_d of 42.5 s, as depicted in **Figure 4a**. The long response time are sacrificed for obtaining ultrahigh photo responsivity. After 5 min ozone treatment, the τ_r and τ_d decline to 1.2 s and 1.5 s, respectively (**Figure 4b**), which is fast enough for special sensing application, i.e. flame sensing [4]. **Figure 4c** shows that the τ_r and τ_d of PDs with longer time ozone treatment (15 min) are lower than 240 ms. The response speed is accelerated with the prolonged oxidation duration, as shown in **Figure 4d.** Compared with other PDs based on organic semiconductors, nanocrystals or other direct bandgap semiconductor, the response speed of the diamond PDs are slower. This is because that it takes time for the N^+ to be neutralized by a part of the photogenerated electrons and for the accumulation of holes under illumination. Whereas, the response wavelength of PDs based on organic semiconductors is around 300 nm~800 nm [48, 49, 50, 51], which cannot meet the requirement of the deep UV light detection. In the future, we would adjust the ozone treatment temperature or use different gases such as water vapor at high temperature [52] to continue to improve the response speed. In general, the photo response regulation is achieved successfully by surface treatments. In other words, by using simple surface treatments, the PD can achieve high responsivity, fast response speed, and high spectral selectivity or tailoring these figure-of-merits to satisfy various application scenarios requiring either high responsivity or fast speed.

In addition to verify the repeatability of the ultra-high performance of other PDs based on the type-Ib diamond with 30 min H-plasma treatment, called device 4, was also characterized, the results of which are shown in **Figure S3 (Supporting Information)**. The similar photoresponse performance was obtained. In addition, a number of devices were measured to analyze the trend of electrical dark current with the ozone treatment duration, as displayed in **Figure S4 (Supporting Information)**. These results enhance support the tunability and reproducibility of the effect of the surface treatments on the photoelectrical behavior of type-Ib diamond. The linear dynamic range (LDR) is a key parameter for PDs to characterize the light intensity range in which the photodetectors have a constant responsivity. The LDR can be calculated by LDR=10log(Psat/Plow) [47]. the LDR of the as-hydrogenated PD, 5 min-ozone oxidized PD, 15 min-ozone oxidized PDs are 48.6 dB, 68.6 dB, and 70.4 dB, respectively, as shown in (**Figure S5 (Supporting Information)**). The trend of LDR is closely related to the dark current, that is, the surface hole carrier concentration. As for the as-hydrogenated PD, both the C-H bonds density and the ionized nitrogen density [N+] which acts as deep traps are the highest, the photocurrent is dominated by the large amount of holes on the diamond surface due to the filling of the photogenerated electrons into the deep N+ traps. Thus, the photoresponse is slow and the photocurrent tends to be saturated under a low power intensity. While as for 15 min-ozone oxidized PD, the C-H bonds density decreases and the C-O or C=O bonds density increases, less with acts as recombination centers, less [N+] in the diamond substrate captures electrons, thus, less corresponding holes on the surface is generated. The photocurrent is dominated by both surface recombination and deep nitrogen traps. Therefore, higher light intensity is required to saturate the hole accumulation. Correspondingly, the response speed is higher. As the diamond surface is fully oxidized, the photo-generation process is dominated by the surface recombination. Thus, the response speed is high. The LDR will be enlarged. Furthermore, to confirm the stability of PDs, time-dependent photoresponse of the PDs was also measured, as shown in **Figure S6 (Supporting Information)**. It can be seen that

the PD current periodically rises and falls as the light source is turned on and off. There is no degradation of the performance after multiple cycle tests, indicating that the PDs have excellent stability.

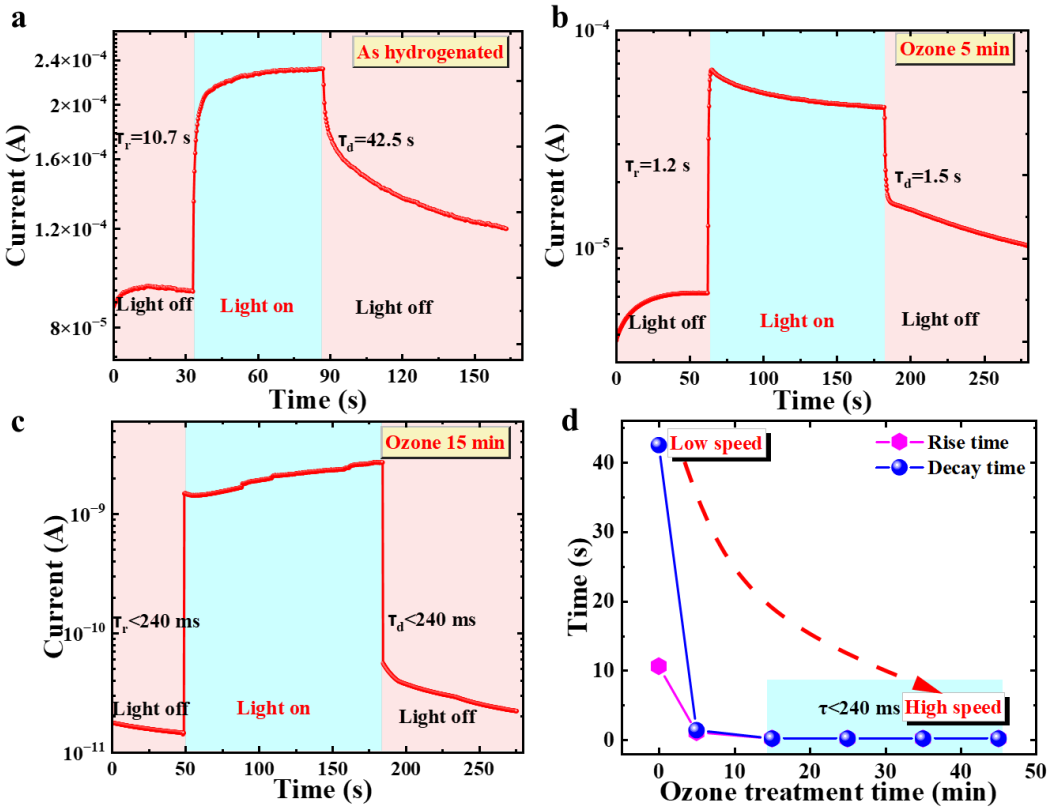

Figure 4. Time-dependent photo-response of PDs. a) As hydrogenated. b) 5 min ozone oxidized. c) 15 min ozone oxidized. d) The dependence of photo-response time of PDs on ozone treatment time.

2.3 Photoconductive mechanism based on synergistic effect of surface states and deep defects

The key performance parameters of the PDs with different surface treatments by hydrogen plasma and ozone treatments are summarized in **Table S1 (Supporting Information)**. The as hydrogenated diamond-based PD is at far advanced level in terms of responsivity, *EQE* and D*. Furthermore, the EQE and response speed of the PDs can be tailored with different surface treatments. In our work, the photo-response of diamond-based PDs is tailored by the synergistic effect of surface adsorbates and deep-defect nitrogen in the bulk diamond: (i) the N^+ traps are

generated by compensating the holes at the surface, (ii) the N^+ are filled with the photo-generated electrons to be neutral nitrogen under illumination, (iii) the holes are accumulated to enhance photoelectric conductance. The mechanism could be clarified through the energy band diagrams shown in **Figure 5**. When the PDs are illuminated under the 220 nm DUV light, electron-hole pairs are generated in the conduction band E_c and valence band Ec, respectively. The density of photogenerated holes ($D(h^+)_{ph}$) is equal to the density of photogenerated electrons ($D(e^-)_{ph}$), as shown in equation (3). Some of the photogenerated electrons fill the N^+, and some remain in the valence band ($D(e^-)_{Ev}$), which can be expressed by equation (4). Here we assume that there is no other bulk defects and surface defects involved to qualitatively explain the experimental observation.

$$D(h^+)_{ph} = D(e^-)_{ph} \quad (3)$$

$$D(e^-)_{ph} = \Delta D(N^+)_{filled} + D(e^-)_{Ev} \quad (4)$$

In the case of hydrogen-terminated type Ib-type diamond-based PDs, the ionized nitrogen (N^+) traps induced by surface air adsorbates on the H-terminated diamond **(Figure 1a)** are filled by the photo-generated electrons from the E_c, resulting in the accumulation of holes, as demonstrated in **Figure 5a**. The accumulation of the holes causes the band to bend upwards more sharply and the photocurrent to increase significantly instead of being buried, corresponding to the ultra-high responsivity (2.5×10^4 A/W) and *EQE* (1.4×10^7 %). The trapping process by photo-generated electrons by the charged N^+ slows down the carrier recombination process due to the deep-energy nature of nitrogen in diamond, thus, resulting in a long decay time. While the PDs after short-time ozone treatment have fewer N^+ traps **(Figure 1b)** and less hole accumulation, as shown in **Figure 5b**. In addition, the ozone treatment may also generate recombination centers, leading to a lower photocurrent and faster speed. **Figure 5c** is the band diagram of the fully O-terminated diamond-based PDs under illumination, which is downward bending. In this case, there is nearly no surface holes in dark, thus nearly no N^+ traps. The

photocurrent is dominated by the surface recombination. Therefore, the EQE is the lowest in this case and the response speed is the highest.

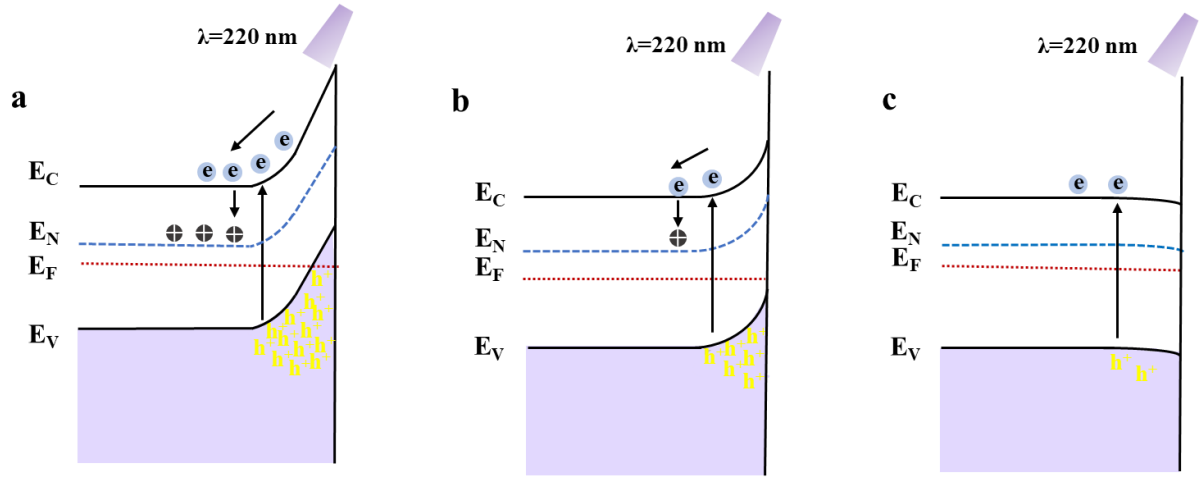

Figure 5. Schematic energy band diagrams of PDs under illumination. a) H-termination. b) partial H-termination. c) O-termination.

2.4 State-of-the-art of solar-blind PDs

The main parameters including the dark current, *R*, *EQE*, and spectral response of PD in this work and previously reported diamond-based PDs, AlGaN-based PDs, Ga_2O_3-based PDs are summarized in **Table 1**. The *R* and *EQE* of this work are far superior to all those of the previously reported diamond-based PDs [27, 32, 33, 41, 53, 54, 55, 56, 57], and even higher than most Ga_2O_3-based PDs [14, 58, 59, 60]and AlGaN-based PDs [61, 62, 63]. Although the reported *R* of *β*-Ga_2O_3/MgO/Nb:$SrTiO_3$ heterostructure-based APD reached 4.46×10^5 A/W, the operating voltage is as high as 78.1 V[12]. The *R* in the present work is similar to those of PMTs and APD. However, the operation voltage of the diamond MSM PD in this work is as low as 5 V. By controlling the surface treatments, the 5S requirements for a photodetector can be tailored to satisfy the specific application requirements. In **Figure 6,** we show the DUV/visible light rejection ratio and DUV responsivity of the present PD based on the H-terminated type-Ib diamond substrate by comparing with those of the reported ones based on other UWBG semiconductors. It can be clearly seen that the PDs based on the hydrogenated type-Ib diamond

has the highest EQE, despite the indirect bandgap structure of diamond. Conventional AlGaN-based PDs without avalanche process exhibit low responsivity and rejection ratio. Usually, the responsivity of direct bandgap Ga_2O_3-based detectors is larger than that of indirect bandgap diamond-based detectors. However, the H-terminated type-Ib diamond-based PDs in this work show larger responsivity and higher rejection ratio than the majority of Ga_2O_3-based PDs. The significant merits of the PDs in this work are the simple surface treatments with short durations of readily accessible commercial type-Ib diamond substrates, no requirements of additional epilayer growth as reported up to now, and the simplest MSM device geometry. The surface conductivity of diamond differs from any other semiconductors, providing a unique feature to tailor the photoelectric properties by combing with the deep defects in the bulk.

Table 1. Comparison of the critical parameters of the DUV PDs based on UWBG semiconductors.

Material	Structure	Dark current	Responsivity (A/W)	EQE (%)	Response time(τr/τd)	Rejection ratio	Ref
SCD	MSM	5×10^{-6} A@50 V	21.8@50 V, 218 nm	1.24×10^{4}	310μs/330μs	8.9×10^{3}	32
SCD	MSM	1.08×10^{-10} A@13 V	524.9@13 V, 220 nm	2.96×10^{5}	0.16 μs/120 μs	2.1×10^{4}	33
SCD	MSM	2.45×10^{-5} A@120 V	56.3@50 V, 213 nm	3.28×10^{4}	1 ns	9.6×10^{3}	53
SCD	MSM	10^{-13} A@43.5 V	1.18@50 V, 210 nm	6.87×10^{2}	640ms/34ms	10^{3}	57
SCD	MSM	10^{-12} A@47 V	0.013@47 V, 225 nm	7.19	5ns/20ns	1.4×10^{4}	54
B-doped SCD	MSM	10^{-12} A@30 V	0.325@30 V, 210 nm	1.92×10^{2}	1.2 ms	10^{4}	55
B-doped SCD	MSM	10^{-12} A@20 V	6@3 V, 220 nm	3.38×10^{3}	10 ns	10^{8}	41
B-doped SCD	MSM	10^{-12} A@30 V	18@-23 V, 220 nm	1.01×10^{4}	<10ms	10^{8}	27
B-doped SCD	Schottky photodiode	10^{-6} A@-10 V	10@2 V, 220 nm	5.6×10^{3}	<1s	10^{6}	56
β-Ga_2O_3	APD	10^{-9} A@-73.2 V	446000@-78.1 V, 254 nm	2.2×10^{8}	12.4ns/41.7μs	-	12
α-Ga_2O_3/ZnO	APD	10^{-6} A@-40 V	11000@-40 V, 254 nm	5.37×10^{6}	238μs	10^{3}	58
β-Ga_2O_3/TiN	MSM	10^{-5} A@15 V	276.7@15 V, 250 nm	1.37×10^{5}	581ms	2×10^{3}	14
ε-Ga_2O_3	MSM	2.35×10^{-11} A@6 V	230@6 V, 254 nm	1.13×10^{5}	24ms	1.2×10^{5}	59
$MoTe_2$/Ta-Ga_2O_3	pn junction	1.78×10^{-9} A@1.5 V	358.9@1.5 V, 254 nm	1.76×10^{5}	21.1ms/84.5ms	1.1×10^{3}	60
AlGaN	MSM	1.2×10^{-11} A@10 V	3.42@10 V, 270 nm	1.57×10^{3}	34.57ms/59.31ms	10^{3}	61
$Al_xGa_{1-x}N$	APD	$<8\times10^{-15}$ A@20 V	0.13@20 V, 272 nm	59.2	-	10^{4}	62
AlGaN	HFEPT	10^{-12} A@10 V	19000@3 V, 272 nm	8.66×10^{6}	4.4ns/0.591ms	1.6×10^{2}	63
H-Ib diamond	MSM	4.2×10^{-5} A@5 V	25024@5 V, 220 nm	1.4×10^{7}	10.7 s/42.5 s	6.7×10^{5}	**This work**
H-Ib diamond (5min ozone)	MSM	4.4×10^{-6} A@5 V	4891@5 V, 220 nm	2.8×10^{6}	1.2 s/1.5 s	7.7×10^{4}	**This work**
H-Ib diamond (15 min ozone)	MSM	7.6×10^{-12} A@5 V	0.29@5 V, 220 nm	1.6×10^{2}	<240 ms	5.4×10^{4}	**This work**

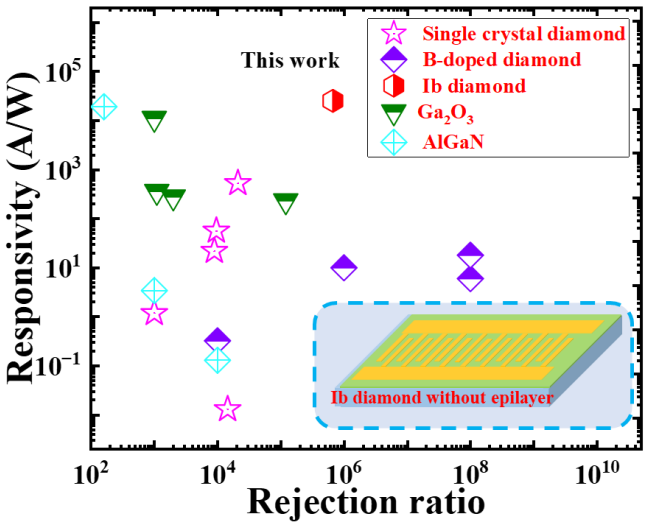

Figure 6. Rejection ratio versus responsivity for PDs based on diamond, Ga_2O_3, and AlGaN.

3. Conclusions

In conclusion, DUV photodetectors with a high gain over 10^5 was achieved at low operation voltage of 5 V by using the synergistic effect of surface states and deep defects in diamond, despite the indirect band structure nature of diamond. The photoresponse performance is comparable with those of APD and PMTs that require much higher operation voltages. Our approach is simply based on the surface terminations of a type-Ib SCD substrate including hydrogen plasma and ozone treatments. The overall photoresponse properties such as the DUV sensitivity, response speed, DUV/visible light rejection ratio, and detectivity of the diamond PDs could be tailored by the surface treatments. The type-Ib diamond-based PDs in this work demonstrate superior and tailored performance, which promises to eliminate the burden of diamond epitaxial layer growth generally required. The surface adsorbates and deep nitrogen defects coordinately tailoring the photo-response opens up a cost-effective strategy for the development of high-performance DUV PDs meeting various scenario requiring either high sensitivity or response speed, such as DUV light monitoring, bio-imaging sensing, and space communication etc.

4. Experimental section

4.1 Device fabrication

The overall experimental process is shown in **Figure 7**. The hydrogen-terminated diamond surface was obtained from a commercial type-Ib (100) single-crystal diamond substate with dimensions of 2.5 mm×2.5 mm×0.5 mm by using hydrogen plasma treatment in a microwave plasma chemical vapor deposition apparatus. The base pressure, working pressure, microwave power and duration are 10^{-8} Torr, 80 mTorr, 400 W and 20 min/30 min, respectively. An ozone ambient was used to oxidize the hydrogen-terminated diamond. The tungsten carbide (WC) interdigitated electrodes were deposited on the type-Ib (100) diamond with a finger width and spacing of 10 μm through a standard photolithography process prior to the ozone oxidation. The metal-semiconductor-metal (MSM) devices were placed in a black box filled with oxygen and exposed to UV light to oxidize the diamond surface. The ozone treatment durations were set as 5 min, 15 min, 25 min,35 min, and 45min.

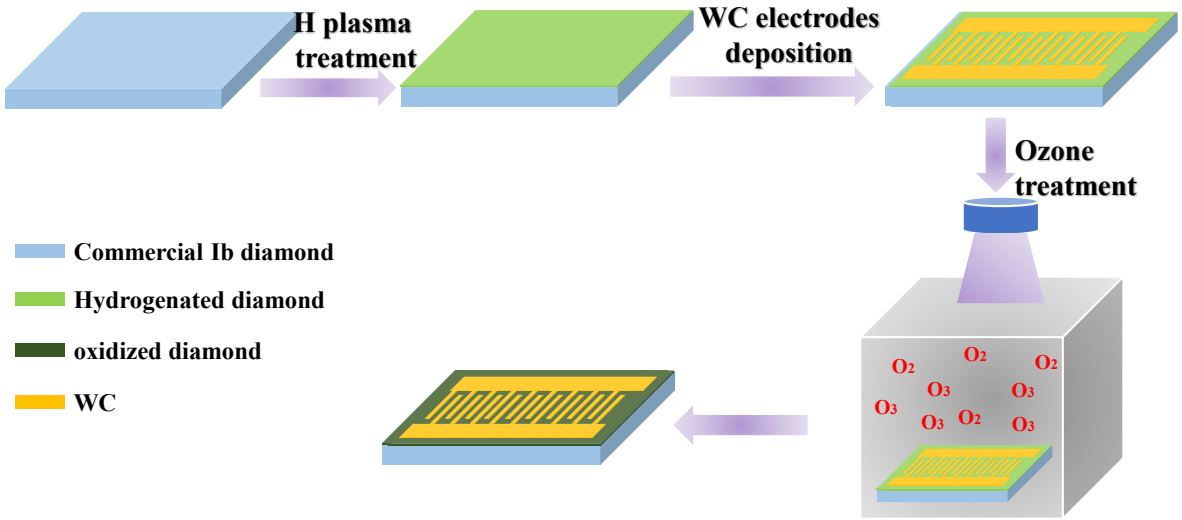

Figure7. Schematic diagrams of the experimental treatment routes.

4.2 Device measurements

The electrical properties of the MSM devices were measured in a two-probe station by a semiconductor analyzed (Advantest). The photocurrent and transient photo-response of the PDs

were examined by a 220 nm DUV light illumination with the intensity of ~20 μW/cm^2. A 500 W Ushio Xenon lamp combined with an Acton monochromator with order sorting filters and a standard lock-in amplifier technique were used to measure the spectral response. The electrical properties were measured after each surface treatment.

Supporting Information

Supporting Information is available from the Wiley Online Library or from the author.

Acknowledgements

This was partially supported by a Grant-in-Aid of JSPS KAKENHI (Grant Numbers 22K18957, 24H00287) of the Ministry of Education, Culture, Sports, and Technology (MEXT) of Japan.

Conflict of Interest

The authors declare no conflict of interests.

References

[1] W. Y. Kong, G. A. Wu, K. Y. Wang, T. F. Zhang, Y. F. Zou, D. D. Wang, L. B. Luo, *Advanced Materials* **2016**, 28, 10725.
[2] J. Chen, W. Ouyang, W. Yang, J. H. He, X. Fang, *Advanced Functional Materials* **2020**, 30, 1909909.
[3] Y. Chen, Y. Li, S. Niu, X. Yang, W. Dou, C. Shan, G. J. A. F. M. Shen, **2024**, 2315383.
[4] M. Liao, *Functional Diamond* **2021**, 1, 29.
[5] L. Yang, D. Yang, D. Guo, J. Zheng, S. Tao, J. Li, G. He, D. J. A. F. M. Ma, **2022**, 32, 2206993.
[6] D. Gedamu, I. Paulowicz, S. Kaps, O. Lupan, S. Wille, G. Haidarschin, Y. K. Mishra, R. J. A. M. Adelung, **2014**, 26, 1541.
[7] D. Shao, W. Zhu, X. Liu, M. Li, J. Chen, Y.-Y. Sun, G. Xin, J. Lian, S. J. A. A. M. Sawyer, Interfaces, **2020**, 12, 43106.
[8] K. Arora, N. Goel, M. Kumar, M. Kumar, *Acs Photonics* **2018**, 5, 2391.
[9] X. Shi, Z. Yang, S. Yin, H. Zeng, *Materials Technology* **2016**, 31, 544.
[10] B. Liu, D. Chen, H. Lu, T. Tao, Z. Zhuang, Z. Shao, W. Xu, H. Ge, T. Zhi, F. J. A. M. Ren, **2020**, 32, 1904354.
[11] C. Xie, X. T. Lu, X. W. Tong, Z. X. Zhang, F. X. Liang, L. Liang, L. B. Luo, Y. C. Wu, *Advanced Functional Materials* **2019**, 29, 1806006.
[12] Q. Zhang, N. Li, T. Zhang, D. Dong, Y. Yang, Y. Wang, Z. Dong, J. Shen, T. Zhou, Y. Liang, W. Tang, Z. Wu, Y. Zhang, J. Hao, *Nature Communications* **2023**, 14, 418.
[13] Q. Cai, H. You, H. Guo, J. Wang, B. Liu, Z. Xie, D. Chen, H. Lu, Y. Zheng, R. Zhang, *Light: Science & Applications* **2021**, 10, 94.

[14] N. Alfaraj, K. H. Li, M. Alawein, C. H. Kang, L. Braic, N. C. Zoita, A. E. Kiss, T. K. Ng, B. S. Ooi, *Advanced Materials Technologies* **2021**, 6, 2100142.
[15] Z. Wang, K. Han, H. Huang, X. Zhao, H. Zhan, X. Hou, X. Feng, X. Zhou, G. Xu, F. J. A. F. M. Zhang, 2400498.
[16] A. Kalra, U. U. Muazzam, R. Muralidharan, S. Raghavan, D. N. J. J. o. A. P. Nath, **2022**, 131.
[17] X. Chen, F. Ren, S. Gu, J. Ye, *Photon. Res.* **2019**, 7, 381.
[18] Z. Peng, X. Hou, Z. Han, Z. Gan, C. Li, F. Wu, S. Bai, S. Yu, Y. Liu, K. J. A. F. M. Yang, 2405277.
[19] F. Capasso, in *Semiconductors and Semimetals*, Vol. 22 (Ed: W. T. Tsang), Elsevier **1985**, p. 1.
[20] Z. G. Shao, D. J. Chen, H. Lu, R. Zhang, D. P. Cao, W. J. Luo, Y. D. Zheng, L. Li, Z. H. Li, *IEEE Electron Device Letters* **2014**, 35, 372.
[21] P. Reddy, M. Hayden Breckenridge, Q. Guo, A. Klump, D. Khachariya, S. Pavlidis, W. Mecouch, S. Mita, B. Moody, J. Tweedie, R. Kirste, E. Kohn, R. Collazo, Z. Sitar, *Applied Physics Letters* **2020**, 116.
[22] S. Shikata, *Diamond and Related Materials* **2016**, 65, 168.
[23] Z. Zhang, H. Wu, L. Sang, J. Huang, Y. Takahashi, L. Wang, M. Imura, S. Koizumi, Y. Koide, M. Liao, *Carbon* **2019**, 152, 788.
[24] Z. Zhang, H. Wu, L. Sang, Y. Takahashi, J. Huang, L. Wang, M. Toda, I. M. Akita, Y. Koide, S. Koizumi, *ACS applied materials & interfaces* **2020**, 12, 23155.
[25] M. Imura, M. Togawa, M. Miyahara, H. Okumura, J. Nishinaga, M. Liao, Y. Koide, *Functional Diamond* **2022**, 2, 167.
[26] Z. Zhai, C. Zhang, B. Chen, Y. Xiong, Y. Liang, L. Liu, B. Yang, N. Yang, X. Jiang, N. J. A. F. M. Huang, **2024**, 2401949.
[27] M. Liao, Y. Koide, J. Alvarez, *Applied physics letters* **2007**, 90, 123507.
[28] M. Liao, Y. Koide, J. Alvarez, *Applied Physics Letters* **2005**, 87, 022105.
[29] Z. Liu, F. Li, S. Li, C. Hu, W. Wang, F. Wang, F. Lin, H. Wang, *Scientific reports* **2015**, 5, 14420.
[30] Y.-C. Chen, Y.-J. Lu, C.-N. Lin, Y.-Z. Tian, C.-J. Gao, L. Dong, C.-X. Shan, *Journal of Materials Chemistry C* **2018**, 6, 5727.
[31] K. Liu, B. Dai, V. Ralchenko, Y. Xia, B. Quan, J. Zhao, G. Shu, M. Sun, G. Gao, L. Yang, *Sensors and Actuators A: Physical* **2017**, 259, 121.
[32] C. N. Lin, Y. J. Lu, X. Yang, Y. Z. Tian, C. J. Gao, J. L. Sun, L. Dong, F. Zhong, W. D. Hu, C. X. Shan, *Advanced Optical Materials* **2018**, 6, 1800068.
[33] C.-N. Lin, Z.-F. Zhang, Y.-J. Lu, X. Yang, Y. Zhang, X. Li, J.-H. Zang, X.-C. Pang, L. Dong, C.-X. Shan, *Carbon* **2022**, 200, 510.
[34] L. Wang, X. Chen, G. Wu, W. Guo, Y. Wang, S. Cao, K. Shang, W. Han, *physica status solidi (a)* **2010**, 207, 468.
[35] M. Bevilacqua, R. B. Jackman, *Applied Physics Letters* **2009**, 95, 243501.
[36] J. Navas, D. Araujo, J. C. Piñero, A. Sánchez-Coronilla, E. Blanco, P. Villar, R. Alcántara, J. Montserrat, M. Florentin, D. J. A. S. S. Eon, **2018**, 433, 408.
[37] H. Kawarada, *Journal of Physics D: Applied Physics* **2023**, 56, 053001.
[38] Z. Ren, S. Ding, Z. Liang, Q. He, K. Su, J. Zhang, J. Zhang, C. Zhang, Y. Hao, *Applied Physics Letters* **2022**, 120, 042104.
[39] K. Kudara, S. Imanishi, A. Hiraiwa, Y. Komatsuzaki, Y. Yamaguchi, Y. Kawamura, S. Shinjo, H. Kawarada, *IEEE Transactions on Electron Devices* **2021**, 68, 3942.
[40] P. K. Ang, K. P. Loh, T. Wohland, M. Nesladek, E. J. A. f. m. Van Hove, **2009**, 19, 109.
[41] M. Liao, Y. Koide, *Applied physics letters* **2006**, 89, 113509.

[42] M. Hauf, B. Grotz, B. Naydenov, M. Dankerl, S. Pezzagna, J. Meijer, F. Jelezko, J. Wrachtrup, M. Stutzmann, F. Reinhard, *Physical Review B* **2011**, 83, 081304.
[43] H. Kawarada, T. Yamada, D. Xu, H. Tsuboi, Y. Kitabayashi, D. Matsumura, M. Shibata, T. Kudo, M. Inaba, A. Hiraiwa, *Scientific reports* **2017**, 7, 1.
[44] X. Zhu, S. Shao, S. Chan, J. Tu, K. Ota, Y. Huang, K. An, L. Chen, J. Wei, J. Liu, *Advanced Electronic Materials* **2023**, 9, 2201122.
[45] V. Petráková, A. Taylor, I. Kratochvílová, F. Fendrych, J. Vacík, J. Kučka, J. Štursa, P. Cígler, M. Ledvina, A. J. A. F. M. Fišerová, **2012**, 22, 812.
[46] K. Liu, S. Zhang, B. Liu, M. Xu, Z. Ren, P. Qiao, J. Xue, X. Zhang, G. Shu, J. Zhao, *Carbon* **2020**, 169, 440.
[47] Y. Xu, Q. J. A. P. R. Lin, **2020**, 7.
[48] F. Guo, Z. Xiao, J. J. A. O. M. Huang, **2013**, 1, 289.
[49] C. Bao, Z. Chen, Y. Fang, H. Wei, Y. Deng, X. Xiao, L. Li, J. J. A. m. Huang, **2017**, 29, 1703209.
[50] Y. Fang, F. Guo, Z. Xiao, J. J. A. O. M. Huang, **2014**, 2, 348.
[51] R. Nie, X. Deng, L. Feng, G. Hu, Y. Wang, G. Yu, J. J. S. Xu, **2017**, 13, 1603260.
[52] R. Yoshida, D. Miyata, T. Makino, S. Yamasaki, T. Matsumoto, T. Inokuma, N. J. A. S. S. Tokuda, **2018**, 458, 222.
[53] M. Feng, P. Jin, X. Meng, P. Xu, X. Huo, G. Zhou, P. Qu, J. Wu, Z. Wang, *Journal of Physics D: Applied Physics* **2022**, 55, 404005.
[54] M. Girolami, V. Serpente, M. Mastellone, M. Tardocchi, M. Rebai, Q. Xiu, J. Liu, Z. Sun, Y. Zhao, V. Valentini, *Carbon* **2022**, 189, 27.
[55] Y. Iwakaji, M. Kanasugi, O. Maida, T. Ito, *Applied Physics Letters* **2009**, 94, 223511.
[56] Y. Koide, M. Liao, J. Alvarez, *Diamond and related materials* **2006**, 15, 1962.
[57] Z. Liu, D. Zhao, J. Ao, X. Chang, Y. Wang, J. Fu, M. Zhang, H. Wang, *Optics Express* **2018**, 26, 17092.
[58] X. Chen, Y. Xu, D. Zhou, S. Yang, F.-f. Ren, H. Lu, K. Tang, S. Gu, R. Zhang, Y. Zheng, *ACS applied materials & interfaces* **2017**, 9, 36997.
[59] Y. Qin, L. Li, X. Zhao, G. S. Tompa, H. Dong, G. Jian, Q. He, P. Tan, X. Hou, Z. Zhang, *Acs Photonics* **2020**, 7, 812.
[60] G. Zeng, M.-R. Zhang, Y.-C. Chen, X.-X. Li, D.-B. Chen, C.-Y. Shi, X.-F. Zhao, N. Chen, T.-Y. Wang, D. W. Zhang, *Materials Today Physics* **2023**, 101042.
[61] W. Li, Y. Wang, G. Gu, F. Ren, D. Zhou, W. Xu, D. Chen, R. Zhang, Y. Zheng, H. J. I. T. o. E. D. Lu, **2023**.
[62] T. Tut, M. Gokkavas, A. Inal, E. J. A. P. L. Ozbay, **2007**, 90.
[63] K. Wang, X. Qiu, Z. Lv, Z. Song, H. J. P. R. Jiang, **2022**, 10, 111.

Table of Contents

Synergistic effect of surface states and deep defects for ultrahigh gain deep-ultraviolet photodetector with low-voltage operation

Keyun Gu[1,2], Kongping Wu[3], Zilong Zhang[1], Jian Huang[2], Yasuo Koide[1], and Meiyong Liao[1*]

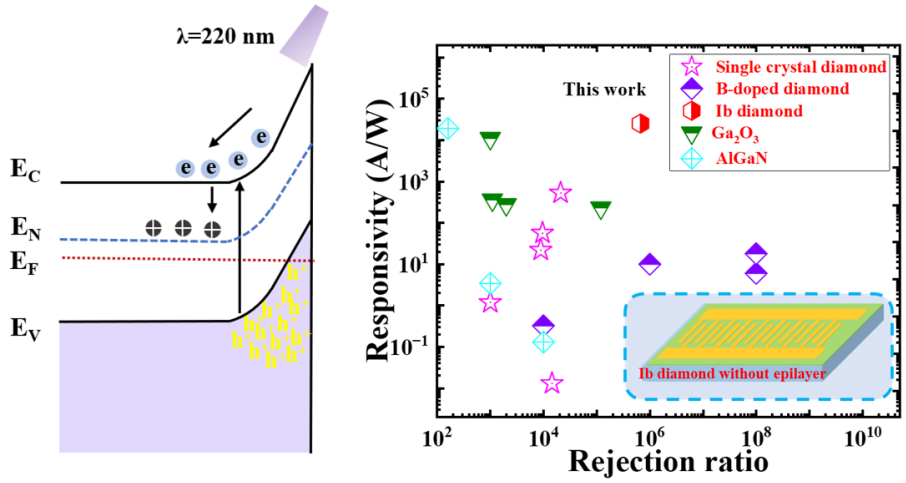

By combing the synergistic effect of surface states and bulk deep defects, deep-ultraviolet photodetectors with ultra-high gain and low-voltage operation are achieved. This work opens up a cost-effective strategy for the development of high-performance ultraviolet detectors meeting various scenario requiring either high sensitivity or response speed.